

КВАНТОВО-ХИМИЧЕСКОЕ И МОНТЕ-КАРЛО МОДЕЛИРОВАНИЕ ЭФФЕКТИВНОСТИ ИНГИБИРОВАНИЯ КОРРОЗИИ 2-МЕРКАПТО-5-ФЕНИЛФУРАНА И БИС(ПИРИДИЛ)ОКСАДИАЗОЛОВ

Д.М. Маманд, Х.М. Кадр

Дьяри Мустафа Маманд (ORCID 0000-0002-1215-7094), Хива Мохаммад Кадр (ORCID 0000-0001-5585-3260)*
Рапаринский университет, Научный колледж, факультет физики, Сулеймания, Ирак, 46012
Email: dyari.mustafa@uor.edu.krd, hiwa.physics@uor.edu.krd*

Теоретические параметры фурана (ингибитор А), 3,5-бис(4-пиридил)-1,2,4-оксидиазола (ингибитор В) и 2,5-бис(2-пиридил)-1,3,4-оксадиазола (ингибитор С) исследовали с использованием теории функционала плотности (DFT) и методов Монте-Карло при базовом наборе 6-311++G(d, p) для протонированных и непротонированных частиц в газовой и водной фазах. Квантово-химические расчеты были проведены для трех гетероциклических соединений, которые использовались в качестве ингибиторов коррозии мягкой стали в кислых средах, чтобы изучить связь между молекулярной структурой ингибитора и эффективностью ингибирования. Энергия и распределение высшей занятой молекулярной орбитали (ВЗМО) и низшей незанятой молекулярной орбитали (НСМО), распределение заряда исследуемых ингибиторов, глобальная мягкость (σ) и жесткость (η), обратное донорство энергии ($\Delta E_{\text{back-donor}}$), электрофильность и нуклеофильность, значения абсолютной электроотрицательности (χ), ширина запрещенной зоны (ΔE_g), потенциал ионизации, химический потенциал и доля переноса электронов (ΔN_{max}) от ингибиторов к мягкой стали также были рассчитаны, которые коррелировали с эффективностью ингибирования. Результаты показали, что эффективность ингибирования ингибиторов улучшалась с увеличением энергии ВЗМО и уменьшением энергетической щели граничной молекулярной орбитали. Вкладывая электроны в мягкую сталь, области с атомами N и O, скорее всего, будут связываться с поверхностью. Расчеты DFT и Монте-Карло использовались для ранжирования трех материалов по антикоррозионным свойствам, и экспериментальные и теоретические результаты были очень похожими.

Ключевые слова: ТФП, метод Монте-Карло, оксадиазолы, коррозия, эффективность ингибирования

QUANTUM CHEMICAL AND MONTE CARLO SIMULATIONS ON CORROSION INHIBITION EFFICIENCY OF 2-MERCAPTO-5-PHENYLFURAN AND BIS(PYRIDYL)OXADIAZOLES

D.M. Mamand, H.M. Qadr

Dyari Mustafa Mamand (ORCID 0000-0002-1215-7094), Hiwa Mohammad Qadr (ORCID 0000-0001-5585-3260)*
University of Raparin, College of Science, Department of Physics, Sulaymaniyah, 46012, Iraq
Email: dyari.mustafa@uor.edu.krd, hiwa.physics@uor.edu.krd*

A theoretical parameters for furan (inhibitor A), 3,5-bis(4-pyridyl)-1,2,4-oxadiazole (inhibitor B) and 2,5-bis(2-pyridyl)-1,3,4-oxadiazole (inhibitor C) were investigated using density functional theory (DFT) and Monte Carlo techniques at 6-311++G(d, p) basis set for protonated and non-protonated species in gas and aqueous phases. Quantum chemical calculations were

done on three heterocyclic compounds which used as mild steel corrosion inhibitors in acid environments to examine the link between inhibitor molecular structure and inhibition performance. Energy and distribution of the highest occupied molecular orbital (HOMO) and lowest unoccupied molecular orbital (LUMO), charge distribution of the studied inhibitors, global softness (σ) and hardness (η), energy back-donation ($\Delta E_{back-donation}$), electrophilicity and nucleophilicity, absolute electronegativity (χ) values, bandgap energy (ΔE_g), ionization potential, chemical potential and the fraction of electrons (ΔN_{max}) transfer from inhibitors to mild steel were also calculated and correlated with inhibition efficiencies. The results indicated that the inhibition efficacy of inhibitors improved with increasing HOMO energy and decreasing energy gap of frontier molecular orbital. By contributing electrons to mild steel, regions with N and O atoms are most likely to bond to the surface. DFT and Monte Carlo calculations were used to rank the three materials for anti-corrosion, and the experimental and theoretical results were very similar.

Key words: DFT, Monte Carlo method, oxadiazoles, corrosion, inhibition efficiency

Для цитирования:

Маманд Д.М., Кадр Х.М. Квантово-химическое и Монте-Карло моделирование эффективности ингибирования коррозии 2-меркапто-5-фенилфурана и бис(пиридил)оксадиазолов. *Изв. вузов. Химия и хим. технология.* 2023. Т. 66. Вып. 8 С. 33–45. DOI: 10.6060/ivkkt.20236608.6807.

For citation:

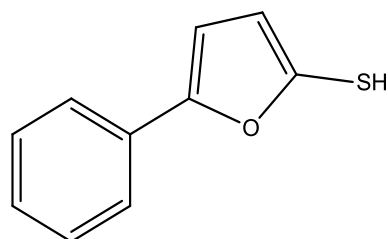
Mamand D.M., Qadr H.M. Quantum chemical and Monte Carlo simulations on corrosion inhibition efficiency of 2-mercapto-5-phenylfuran and bis(pyridyl)oxadiazoles. *ChemChemTech [Izv. Vyssh. Uchebn. Zaved. Khim. Khim. Tekhnol.]*. 2023. V. 66. N 8. P. 33–45. DOI: 10.6060/ivkkt.20236608.6807.

INTRODUCTION

In recent years, corrosion inhibitors have risen significantly due to a greater corrosion consciousness globally. Inhibitors serve a significant function in metal corrosion control. Organic compounds are frequently utilized as corrosion inhibitors in a variety of sectors to avoid damage in acidic conditions [1, 2]. Organic compounds' corrosion inhibition effectiveness (IE) is linked to their adsorption capabilities [3-5]. The adsorption of the inhibitor protects the metal from the corrosive media. It has been discovered that the presence of π -electrons and heteroatoms causes higher adsorption of the adsorbates onto the interface of mild steel [6-8]. As a result, the use of corrosion inhibitors has risen significantly. The bulk of well-known inhibitors are derived from molecules containing heteroatoms like oxygen, nitrogen, or sulfur, along with numerous bonds that promote adsorption on metal surfaces. In any instance, adsorption occurs across a metal surface, an adsorption layer is formed which protects the metal from corrosion [9-13]. These inhibitors' efficacy can be due to their strong polarizability and reduced electronegativity, these inhibitors cover vast metallic surfaces and quickly transfer electrons to atoms' vacant orbitals [6, 7, 14]. Furthermore, organic inhibitors containing nitrogen are effective anticorrosion

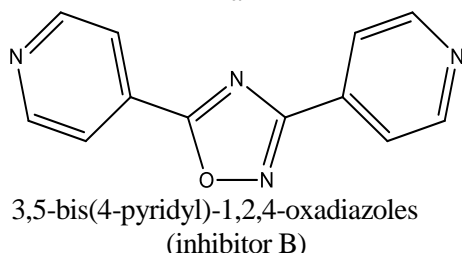
compounds for metals in hydrochloric acid, but molecules that consist of sulfur atoms are effective inhibitors in sulfuric acid [15, 16]. Heterocyclic nitrogen and sulfur act as excellent corrosion inhibitors in both mediums. The activity of any inhibitor in severe acidic conditions on any particular metallic composition relies on the nature of the distinctive inhibitor film deposited on the metal surface, as well as the quantity and kind of adsorption centers donating to the adsorption process [17, 18]. In general, the inhibition efficiency of inhibitors with various heteroatoms reflects the opposite order of their electronegativities, such that inhibition efficiency proceeded in the sequence of $O < N < S < P$ in S, N, O and P [5, 7, 19]. Moreover, theoretical chemistry such as quantum chemical computations has been utilized to elucidate the process of corrosion inhibition. Quantum chemical calculations have shown to be a very effective method for researching the process [20, 21]. The goal of this paper is to offer a theoretical investigation of the electronic and molecular structures of three heterocyclic compounds (Figure 1), as well as to identify the link between both the chemical constituents' molecular structure and inhibitory efficacy. Energy and distribution of the HOMO and LUMO, charge distribution of the studied inhibitors, global softness and hardness, absolute electronegativity (χ) values,

electrophilicity, nucleophilicity, the fraction of electrons (N) transfer from inhibitors to mild steel and energy back-donation were also calculated and correlated with inhibition efficiencies.



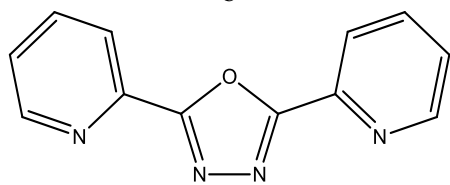
2-mercapto-5-phenylfuran (inhibitor A)

a



3,5-bis(4-pyridyl)-1,2,4-oxadiazoles (inhibitor B)

b



2,5-di(pyridin-2-yl)-1,3,4-oxadiazole (inhibitor C)

c

Fig. 1. Chemical structures of selected compounds a) 2-mercapto-5-phenylfuran (inhibitor A); b) 3,5-bis(4-pyridyl)-1,2,4-oxadiazoles (inhibitor B); c) 2,5-di(pyridin-2-yl)-1,3,4-oxadiazole (inhibitor C)

Рис. 1. Химическая структура выбранных соединений а) 2-меркапто-5-фенилфуран (ингибитор А); б) 3,5-бис(4-пиридил)-1,2,4-оксадиазола (ингибитор В); в) 2,5-ди(пиридин-2-ил)-1,3,4-оксадиазол (ингибитор С)

COMPUTATIONAL DETAIL

For the prediction of the chemical interaction of clusters, solids and molecules, the density functional theory (DFT) has a wide range of user's methodology. In recent decades, DFT has become more popular. In this study, all calculations were performed by Gaussian09 software and material studio [22, 23]. Based on DFT and Becke's three parameters hybrid exchange-correlation functional (B3LYP) were used for obtaining the title molecule's geometry optimizations. The 6-311++ G(d,p) basis set was used in this work. This basis set gives more accurate results for the determination of geometries and electronic properties for a wide range of organic compounds.

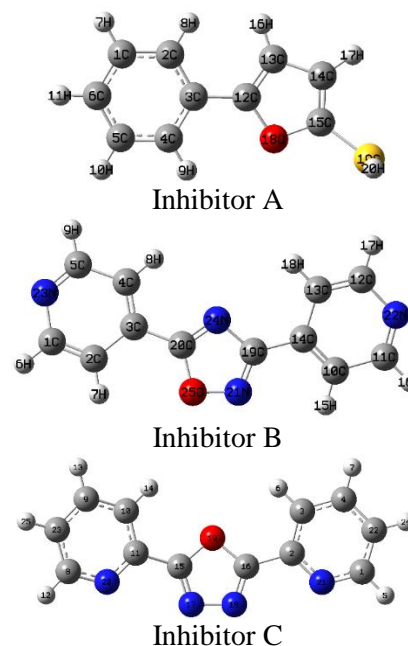


Fig. 2. Optimized chemical structure of selected oxidiazoles
Рис. 2. Оптимизированная химическая структура выбранных оксадиазолов

QUANTUM COMPUTATIONAL CALCULATIONS

Quantum chemical computations were used to study the influence of structural features on inhibitor efficacy and metal surface adsorption mechanisms [24]. By optimizing the inhibitor structure, geometrical and electrostatic structures of the inhibitors were calculated. Fig. 2 shows the optimal structure, bond lengths and Mulliken charges. Frontier orbital theory can be used to anticipate the adsorption centers of inhibitor compounds that interact with surface metal atoms. Due to the reciprocal dependency between stabilization energy and orbital energy difference, frontier MO might contribute significantly. Furthermore, the energy difference between the molecules' HOMO and LUMO regions was a significant aspect to discuss. Excellent corrosion inhibitors are said to be chemical molecules that not only give electrons to the metal's empty orbital but also take free electrons from the metal [25]. The energy of HOMO is frequently related to the molecule's propensity to transfer electrons. Maximum levels of E_{HOMO} are considered to indicate a molecule's proclivity to donate electrons and to suitable acceptor molecules with low energy and unoccupied molecular orbitals [20]. As a result, the energy of LUMO reflects the molecule's capacity to receive electrons [26]. As a result, the lower the value of E_{LUMO} , the more likely the molecule is to receive electrons. The inhibitor's capacity to attach to the metal surface rises with increased HOMO and LUMO energy levels. Because electrochemical corrosion usually comes in the aqueous phase, the impact of solvent must be included in

the computations. As a result, the polarizable continuum method (PCM) was used to account for the influence of the solvent (water) in the computations [27]. For a clearer appreciation of the experimental data obtained from the aqueous solution, the self-consistent reaction field (SCRF) theory and Tomasi's polarized continuum model (PCM) were used [28, 29]. Indicators of global electronics inside the DFT of Parr, Pearson and Yang are valuable tools for analyzing molecular reactivity in ground state. Several parameters can be employed as global or local reactivity characteristics [30].

Within the DFT, lobar hardness (η) evaluates an atom's resistance to charge transfer as the second derivative of the energy gap concerning N at the $v(r)$ property [3].

$$\eta = -\left(\frac{\partial^2 E}{\partial N^2}\right)_{v(r)} \quad (1)$$

Electronegativity is the ability of a set of atoms to attract electrons when chemically bonded with another atom, as expressed by equation 2. Where E indicates the electronic energy, $v(r)$ is the external potential generated by the nuclei and N is the number of electrons [31, 32].

$$\chi = -\left(\frac{\partial E}{\partial N}\right)_{v(r)} \quad (2)$$

Working equations for calculating may be constructed using the finite difference approach as.

$$\chi = \frac{I+A}{2} \quad (3)$$

$$\eta = \frac{I-A}{2} \quad (4)$$

Where A and I are the electron affinity and ionization potential. With the band gap energy value, both I and A can be calculated by the following equations [33].

$$A = E_N - E_{N+1} \quad (5)$$

$$I = E_{N-1} - E_N \quad (6)$$

Where E_N , E_{N+1} and E_{N-1} are the ground state energies of the system with N , $(N + 1)$ and $(N - 1)$ electrons.

Electrons move from the lesser electronegativity compound to the greater electronegativity metal during the interaction of the functional group with bulk metal till the chemical potential is balanced. The proportion of the transported electron, N , was calculated using equation 7.

$$\Delta N = \frac{\chi_m - \chi_i}{2(\eta_m + \eta_i)} \quad (7)$$

Where the indices i and m indicate the inhibitor molecule and metal atom, respectively. χ_i and χ_m represent the absolute electronegativity of iron and the inhibitor molecule, respectively. η_i and η_m represent the absolute hardness of inhibitor molecule and iron, respectively. The theoretical values of χ_m and η_m were

used for bulk iron at 7 eV/mol and 0 eV/mol, using an assumption for a metallic bulk $I = A$. The value of 7.0 eV corresponds to the Fermi energy of iron in the free electron gas model. The electron-electron interaction is ignored, and thus the usage of this number as m is theoretically incorrect [26]. As a result, several studies established that a metal surface's work functions (φ_m) are a good parameter of its electronegativity and should be employed in the calculation of N , as follows [34].

$$\Delta N = \frac{\varphi_m - \chi_i}{2(\eta_m + \eta_i)} \quad (8)$$

The initial molecule-metal interaction energy is an important parameter of molecule, which has been calculated by Sastri and Perumareddi [35].

$$\Delta\psi = \frac{(\chi_{Fe} - \chi_i)^2}{4(\eta_{Fe} + \eta_i)} \quad (9)$$

RESULTS AND DISCUSSION

The examination of the frontier molecular orbitals (FMO) in terms of interaction between the frontier orbitals, including HOMO and LUMO, was used to explore the global molecular reactivity [36]. The energy of HOMO indicates the molecule's capacity to donate electrons. As a result, inhibitors with strong E_{HOMO} values tend to transfer electrons to a suitable acceptor with a low unoccupied molecular orbital energy (MOE). On the other hand, the energy of LUMO reflects the molecule's capacity to receive electrons. The lower the value of E_{LUMO} , the greater likely the molecule is to receive electrons [37]. The efficacy of inhibition rises as E_{HOMO} levels rise. High E_{HOMO} values imply that the compound preferentially donates electrons to compounds having a low-energy empty molecular orbital. The smaller the value of E_{LUMO} , the easier the molecule receives electrons from donor compounds [38, 39]. The obtained value of E_{HOMO} and E_{LUMO} for the examined furan and oxadiazoles for protonated and non-protonated species in gas and aqueous phases are shown in Tables 1-3. The arrangement for the change of inhibition efficiency of the examined inhibitors (for both gas and aqueous phases) is compatible with the order determined from experimental data ($C > B > A$).

When considering structural stability and reactivity, absolute hardness is a critical characteristic. Soft molecules are more reactive than hard molecules since they can easily give electrons [40]. Consequently, inhibitors with the lowest global hardness values are expected to be excellent corrosion inhibitors for noble metals in acidic conditions. Adsorption of inhibitor is a crucial characteristic onto a metallic surface and happens in the softest and hardest region of the molecule [41]. Furthermore, Tables 1-3 show the predicted values of the selected organic molecules as inhibitors in

aqueous and gas phases for protonated and non-protonated species. The findings demonstrate that inhibitors B and A have the highest hardness levels when compared to inhibitor C.

The electronegativity of an atom in a molecule reflects its proclivity to attract electrons. Because excellent inhibitors are often susceptible to donating electrons to the metallic surface, we anticipated that electronegativity values would fall as inhibitive efficiency increased [42]. Furthermore, the values of electronegativity for the current system are compiled in Tables 1-3. The trend in the electronegativity values for the aforementioned inhibitors reveals that inhibitor A has the lowest electronegativity. When compared to inhibitors C and B, this action boosts its adsorption on the mild steel surface and hence improves its corrosion prevention performance.

Tables 1-3 also compute and tabulate the number of electrons transported (ΔN) for non-protonated and protonated species, correspondingly. A positive number of electrons transmitted (ΔN) implies that the molecules are electron donors, whereas a negative number of (ΔN) shows that the molecules are electron acceptors [43]. As a result, in the aqueous and gas medium, in non-protonated species inhibitor C operate as electron donors. If (ΔN) is smaller than 3.6, the inhibition effectiveness is improved by enhancing the inhibitor's electron-donating capacity at the metal surface. Furthermore, the higher the value of (ΔN), the more likely a molecule is to give electrons to the electron-poor species [44, 45]. The inhibitor C has an electron transfer of more than 3.6, suggesting that it acts as an electron acceptor in non-protonation. However, in protonation, it acts as a donor in both gas and solvent because it is less than 3.6. We found that the most acceptable inhibitor C is related with the maximum number of electrons transferred (ΔN_{max}) while the least fraction is associated with the inhibitor with the least inhibitory effect A.

Corrosion of materials in nature for whatever reason is directly related to band gap energy. The energy gap is a crucial characteristic of the inhibitor substance's receptivity to adsorption on the metallic surface [46]. Increasing the band gap energy leads to decrease the reactivity of the molecule. Because the nuclear ionization energy of an atom of the molecule required to remove an electron from the final occupied orbit is minimal. Organic materials are the most suitable corrosion inhibitors because they do not only give electrons to the metal's empty orbit but also take free electrons from the metal. Any material with a low band gap boosts its polarization ability because it increases

chemical activity while decreasing kinetic stability, making it act like soft material [47]. The organic compounds in this study have been theoretically estimated for several quantum chemical characteristics, and according to the band gap energy ranking, the inhibitor A have the worst degree of corrosion, the inhibitor C have greater capacity than other. Fig. 3 shows LUMOs and HOMOs of selected molecules at 6-311++G(d,p) basis set in gas and aqueous phases.

Table 1
Theoretical calculation of electronic parameters for inhibitor A at 6-311++G(d,p) basis set for protonated and non-protonated species in gas and aqueous phases
Таблица 1. Теоретический расчет электронных параметров ингибитора А при базисе 6-311++G(d,p) для протонированных и непротонированных частиц в газовой и водной фазах

Inhibitor A	Non-protonated gas phase	Protonated gas phase	Non-protonated aqueous phase	Protonated aqueous phase
HOMO (eV)	-8.031	-6.351	-8.959	-7.760
LUMO (eV)	-5.522	-1.556	-2.290	-2.686
HOMO-1 (eV)	-8.720	-7.322	-9.30	-8.046
LUMO+1 (eV)	-5.231	-0.701	-2.992	-1.251
Total energy (a.u)	-858.922	-859.224	-859.225	-858.870
Dipole moment (Debye)	3.954	2.826	3.737	4.999
Ionization energy (eV)	9.031	6.351	8.959	8.959
Electron affinity (eV)	4.992	1.556	2.290	3.290
Band-gap energy (eV)	4.039	4.795	6.668	5.668
Hardness (eV)	2.019	2.397	3.334	2.834
Softness (eV)	0.495	0.417	0.299	0.352
Electronegativity (eV)	7.011	3.953	5.625	6.125
Chemical potential (eV)	-7.011	-3.953	-5.625	-6.125
Electrophilicity (eV)	12.172	3.260	4.744	6.618
Nucleophilicity (eV)-1	0.082	0.306	0.210	0.151
ΔE Back-donation (eV)	-0.504	-0.599	-0.833	-0.708
Transfer electrons	-0.002	0.635	0.206	0.154
$ \Delta\Psi $	$-1.7 \cdot 10^{-5}$	-0.967	-0.141	-0.067

Table 2

Theoretical calculation of electronic parameters for inhibitor B at 6-311++G(d,p) basis set for protonated and non-protonated species in gas and aqueous phases

Таблица 2. Теоретический расчет электронных параметров ингибитора В при 6-311++G(d,p) базисном наборе для протонированных и непротонированных частиц в газовой и водной фазах

Inhibitor B	Non-protonated gas phase	Protonated gas phase	Non-protonated aqueous phase	Protonated aqueous phase
HOMO (eV)	-8.886	-8.882	-7.415	-7.584
LUMO (eV)	-5.374	-5.390	-2.822	-3.678
HOMO-1 (eV)	-9.544	-9.553	-7.512	-8.032
LUMO+1 (eV)	-5.178	-5.192	-2.095	-2.864
Total energy (a.u)	-756.129	-755.809	-756.223	-755.963
Dipole moment (Debye)	6.947	3.402	4.385	19.026
Ionization energy (eV)	8.886	8.882	7.415	7.584
Electron affinity (eV)	5.374	5.390	2.822	3.678
Band-gap energy (eV)	3.511	3.492	4.593	3.906
Hardness (eV)	1.755	1.746	1.296	1.953
Softness (eV)	0.569	0.572	0.435	0.511
Electronegativity (eV)	7.130	7.136	5.119	5.631
Chemical potential (eV)	-7.130	-7.136	-5.119	-5.631
Electrophilicity (eV)	14.479	14.58093	5.704	8.117813
Nucleophilicity (eV)-1	0.069	0.068583	0.175	0.123
ΔE Back-donation (eV)	-0.438	-0.436	-0.574	-0.488
Transfer electrons	-0.037	-0.039	0.409	0.350
$ \Delta\Psi $	-0.0024	-0.002	-0.385	-0.239

The dipole moment is a useful indicator for predicting the direction of a corrosion inhibition process. The dipole moment is an estimate of the polarity in a bond and is connected to the diffusion of electrons in a molecule. Although the research is divided on the use as a predictor of the direction of a corrosion inhi-

bition response, it is widely acknowledged that adsorption of polar chemicals with large dipole moments on the metal surface should result in improved inhibition effectiveness [47]. A comparison of quantum chemical calculation results with experimental inhibition efficiency revealed that the percent inhibition efficiencies of the inhibitors rise with increasing dipole moment value. The ranking of the most discussed anti-corrosion agents for the materials in this study according to dipole moment is as follows $A < B < C$.

Table 3

Theoretical calculation of electronic parameters for inhibitor C at 6-311++G(d,p) basis set for protonated and non-protonated species in gas and aqueous phases

Таблица 3. Теоретический расчет электронных параметров ингибитора С при базисе 6-311++G(d,p) для протонированных и непротонированных частиц в газовой и водной фазах

Inhibitor C	Non-protonated gas phase	Protonated gas phase	Non-protonated aqueous phase	Protonated aqueous phase
HOMO (eV)	-5.525	-10.232	-5.477	-7.064
LUMO (eV)	-5.239	-9.775	-5.162	-6.666
HOMO-1 (eV)	-7.335	-11.214	-7.356	-8.132
LUMO+1 (eV)	-2.639	-6.595	-2.638	-3.370
Total energy (a.u)	-754.756	-754.517	-754.776	-754.594
Dipole moment (Debye)	9.474	7.308	9.276	26.868
Ionization energy (eV)	5.525	10.232	5.477	7.064
Electron affinity (eV)	5.239	9.775	5.162	6.666
Band-gap energy (eV)	0.285	0.456	0.315	0.398
Hardness (eV)	0.142	0.228	0.157	0.199
Softness (eV)	7.006	4.385	6.347	5.023
Electronegativity (eV)	5.382	10.004	5.320	6.865
Chemical potential (eV)	-5.382	-10.004	-5.320	-6.865
Electrophilicity (eV)	101.496	219.443	89.830	118.401
Nucleophilicity (eV)-1	0.009	0.004	0.011	0.008
ΔE Back-donation (eV)	-0.035	-0.057	-0.039	-0.049
Transfer electrons	5.666	-6.586	5.330	0.337
$ \Delta\Psi $	-4.582	-9.893	-4.476	-0.022

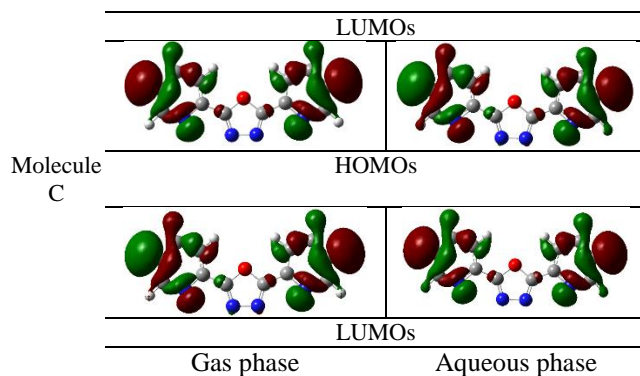
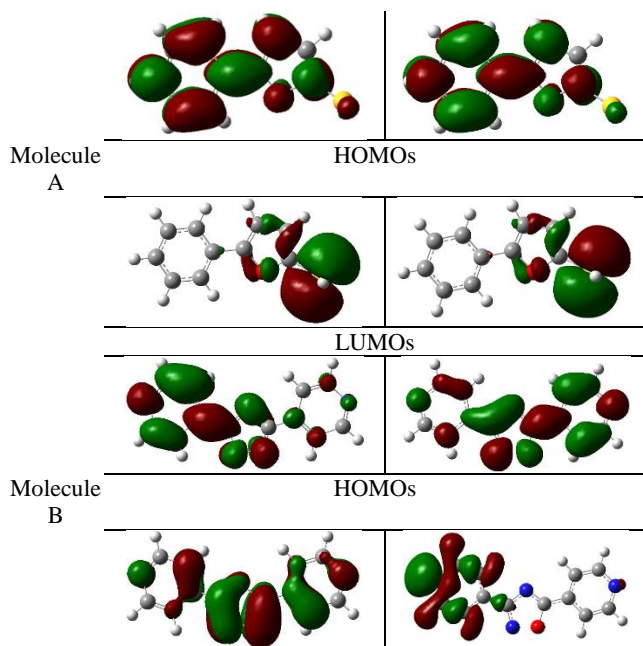


Fig. 3. LUMOs and HOMOs of selected molecules calculated based on DFT at non-protonated species on B3LY level at 6-311++G(d,p) basis set at gas and aqueous phases
 Рис. 3. HСМО и ВЗМО выбранных молекул, рассчитанные на основе DFT для непротонированных молекул на уровне B3LY при базе 6-311++G(d,p) для газовой и водной фаз

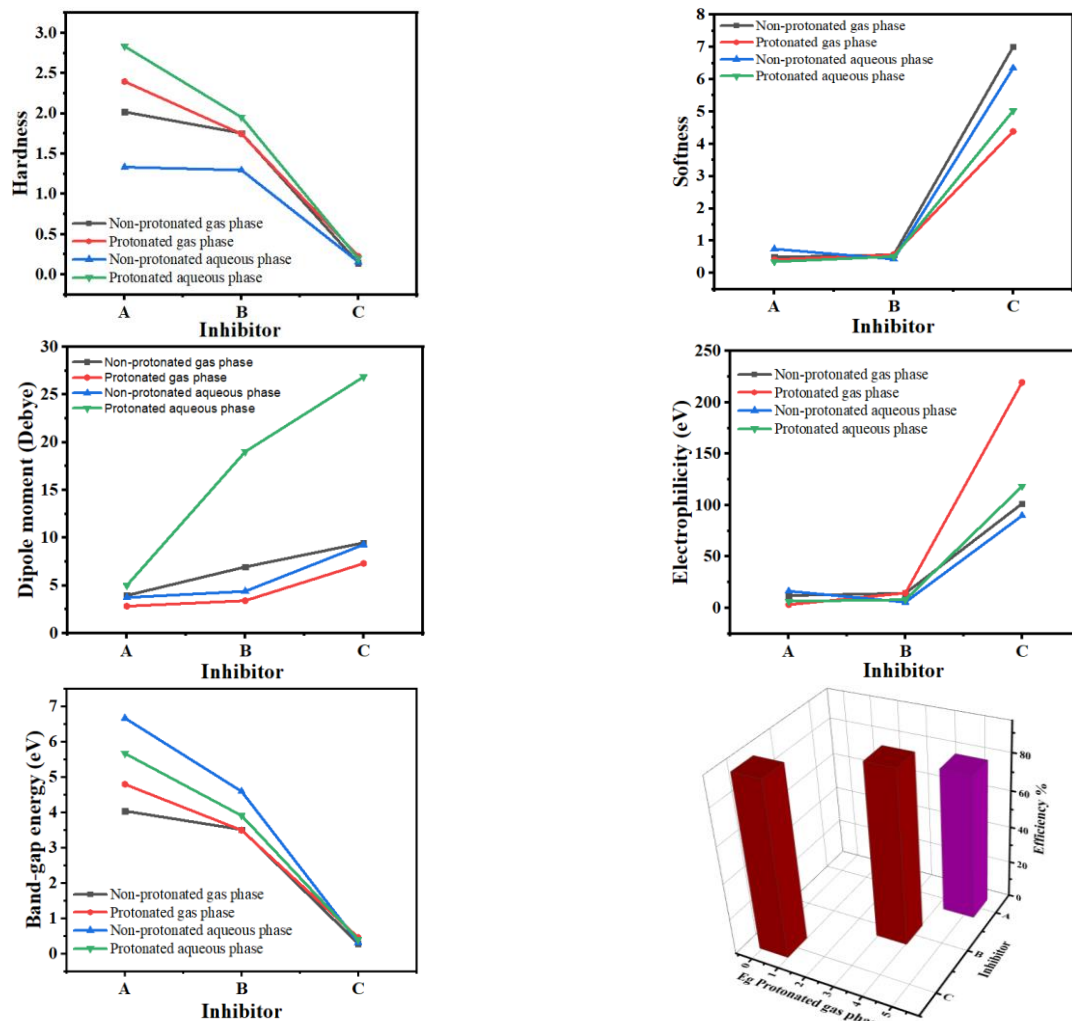


Fig. 4. Variation of quantum chemical parameters in protonated and non-protonates species at gas and aqueous phases with the nature of the inhibitors A, B and C

Рис. 4. Изменение квантово-химических параметров протонированных и непротонированных частиц в газовой и водной фазах в зависимости от природы ингибиторов А, В и С

Electrophilicity and nucleophilicity are quantum chemical factors that can be used to predict the chemical properties of compounds and to compare the efficiencies of inhibitory compounds. It should be noted that a molecule with a high electrophilicity value is useless for corrosion protection [48]. A chemical compound with a high degree of nucleophilicity is, on either side, an effective corrosion inhibitor. $C > B > A$ is the predicted ranking of the corrosion inhibition efficiency based on the electrophilicity and nucleophilicity values of the examined compounds. Another important parameter is back donation energy, can be calculate from the following expression [49].

$$\Delta E_{Back-donation} = -\frac{\eta}{4} \quad (10)$$

The charge transfer model is a successful model for interpretation of charge donation and back-donation, an electronic back-donation mechanism might also influence the chemical interaction between the inhibitor molecule and the metal surface [50]. According to this principle, if both electron transfer to the molecule and back-donation from the compound happen at the same time. Back-donation from the molecule to metal is energetically favored when $\Delta E_{b-d} < 0$ or $\eta > 0$. The findings of this study as given in Tables 1-3 demonstrate that charge transfer to a structure accompanied by back-donation from the molecule is energetically favorable. If molecule corrosion inhibition effectiveness grows with increased molecule adsorption on the metal surface, inhibition efficiency should increase as the stabilization energy arising from the contact between the metal surface and inhibitor increases. The estimated ΔE_{b-d} values show the trend, as predicted and in agreement with the experimental result $C > B > A$.

Organic substances with electronegative functional groups and π -electrons in conjugated double bonds are the most effective inhibitors. Corrosion inhibitors' structural and electrical features have a significant impact on how effective they are. Through their adsorption at the metal/solution interaction, metals are protected against corrosion in acidic environment. The protonation of imidazole and its derivatives leads to an increase in their ability to accept the electrons from the conduction band of the protected metal. The effectiveness of the oxadiazoles and phenylfuran inhibitors, that work by adsorbing on the metal surface, is highly dependent on their capacity to form complexes with the metal. The chelating center for chemical adsorption is provided by the polar functional groups including oxygen and nitrogen as well as the electrons. Organic compounds with various donor atoms have higher inhibitory potencies in the order $N > O$.

However Due to the nitrogen (N) atomic functional groups and free electrons in its N atom's ability

to interact with carbon steel and prevent corrosion attacks, imidazole has the ability to be used as corrosion inhibitors. Put compared our study compounds it has least effective one due to, it has the least molecular size and it has only 1N atoms. so through the nitrogen atom and interactions between aromatic rings, the inhibitor is absorbed on the metal surface. The protective layer is increased by intermolecular hydrogen bonding. It is significant to note that there are no differences in the inhibitors' neutral form's properties in the gas phase. On the other hand, the protonated form was formed during the aqueous phases. The protected metal's ability to accept electrons from the conduction band is enhanced by protonation. During the protonation reaction, their electron cloud is deformed, which improves their capacity to prevent corrosion.

FUKUI FUNCTION ANALYSIS

The Fukui function indicates the reactive centers inside the molecules which was used to examine the local reactivity. The condensed Fukui functions were derived using a finite difference approach as an atom k in a molecule with N electrons [36]. The active sites of the molecules can be found by taking factors that made elements into account: Fukui functions, natural atomic charge and frontier molecular orbital distribution. Many molecular characteristics are dependent on intermolecular interactions, according to the theory of classical chemistry [51, 52]. By definition, all chemical interactions are either orbital (covalent) or electrostatic (polar). Electrostatic interactions are clearly driven by electrical charges in the molecule. Local electric densities or charges are significant in many different compound processes as well as the chemical and physical characteristics of substances [53]. To determine the reactive sites for a particular inhibitor, it is necessary to consider the partial charges on the individual atoms in a molecule. Atoms with the largest negative charge are thought to have the greatest proclivity to donate electrons to the metal surface. As a result, the inhibitor is likely to get involved with the metal surface via these atoms [36]. Fukui function analysis was used for this aim which was used to calculate net atomic charges. Tables 4-6 summarize the atomic charges on the atoms of the selected oxadiazoles in gas and aqueous phases. The atom with the greatest $F^+(r)$ value is the target for nucleophilic assault (r). In turn, the site for electrophilic attack is positioned on the atom with the greatest $F^-(r)$ value. Tables 4-6 provide the values of the Fukui functions for the three oxadiazole compounds [54].

$$F^+(r) = q_k(N) - q_k(N + 1) \quad (11)$$

for nucleophilic attack

$$F^-(r) = q_k(N - 1) - q_k(N) \quad (12)$$

for electrophilic attack

Because N and O heteroatoms have a greater negative charge, they are the most attractive locations for contact with the metal surface for both non-protonated and protonated species, implying that active centers with up with high might operate as a nucleophilic group. The metal's capacity to bind to the inhibitor is highly influenced by the electrical charge of the active site. Each inhibitor compound was given the opportunity to engage with the Fe metal at the atom with the largest negative charge.

Table 4

Calculated Mulliken atomic charges and Fukui functions for inhibitor A and maxima in bold, in gas and aqueous phases

Таблица 4. Расчетные атомные заряды Малликена и функции Фукуи для ингибитора А и максимумы, выделенные жирным шрифтом, в газовой и водной фазах

Atoms	Gas phase			Aqueous phase		
	f^+	f^-	f^0	f^+	f^-	f^0
C1	0.246	-0.227	0.0095	0.001	-0.143	-0.071
C2	0.912	-0.774	0.069	0	-0.094	-0.047
C3	-1.043	1.262	0.1095	0.001	-0.049	-0.024
C4	-0.151	0.204	0.0265	0	-0.101	-0.0505
C5	0.118	-0.029	0.0445	0	-0.15	-0.075
C6	0.106	0.136	0.121	0	-0.117	-0.0585
C12	-0.347	0.487	0.07	0.002	0.292	0.147
C13	0.414	-0.247	0.0835	0.006	-0.33	-0.162
C14	-0.431	0.579	0.074	0.009	-0.256	-0.1235
C15	0.326	-0.258	0.034	0.04	0.252	0.146
O18	-0.57	0.617	0.0235	0.014	0.073	0.0435
S19	1.154	-0.488	0.333	0.927	0.231	0.579

According to the findings, the favored locations for attack by nucleophilic agents in all three inhibitors are around carbon, nitrogen, oxygen and Sulphur atom. Carbons 15 and 16 contain all three states for electrophilic attack and nucleophilic attack which are the most abundant in this molecule while being the best material for the highest corrosion resistance. Carbon positions 15 and 16 are located in the 1,3,4-oxadiazole group. Inhibitor B has a gas-phase active center and is hydrophilic at the heterocyclic atoms. N21, N24 and O25 have nucleophilic attack sites in the 1,3,4-oxadiazole group. When an electron-rich species (the nucleophile) "attacks" an electron-deficient species, this is known as a nucleophilic attack. The inhibitor A like to be attacked by electrophilic substance near the S19 and C1 atoms. The maxima of the electrophilic Fukui functions f^- represent the preferred locations for electrophilic agent adsorption such as metal surfaces. The f^- maxima for inhibitor A, B, and C occur around sites C14, C19 and C20, C14 and C15, respectively.

Table 5

Calculated Mulliken atomic charges and Fukui functions for inhibitor B and maxima in bold, in gas and aqueous phases

Таблица 5. Расчетные атомные заряды Малликена и функции Фукуи для ингибитора В и максимумы, выделенные жирным шрифтом, в газовой и водной фазах

Atoms	Gas phase			Aqueous phase		
	f^+	f^-	f^0	f^+	f^-	f^0
C1	-0.935	0.011	-0.462	0.002	0.044	0.023
C2	0.881	-0.191	0.345	0.007	0.072	0.0395
C3	0.012	0.014	0.013	0	-0.006	-0.003
C4	0.495	-0.289	0.103	0.005	0.063	0.034
C5	-0.721	0.118	-0.3015	0.003	0.048	0.0255
C10	1.807	-0.31	0.7485	-0.026	0.039	0.0065
C11	-0.93	0.105	-0.4125	0.189	0.012	0.1005
C12	-0.673	0.006	-0.3335	0.19	0.018	0.104
C13	-0.33	-0.21	-0.27	-0.025	0.021	-0.002
C14	0.207	0.055	0.131	0.064	-0.009	0.0275
C19	-0.439	0.314	-0.0625	0.022	0.044	0.033
C20	-0.691	0.446	-0.1225	0.007	0.098	0.0525
N21	-0.113	0.053	-0.03	0.025	0.114	0.0695
N22	0.423	-0.152	0.1355	0.173	0.02	0.0965
N23	0.401	-0.12	0.1405	0.003	0.063	0.033
N24	0.583	-0.277	0.153	0.004	0.069	0.0365
O25	0.68	0.177	0.4285	0.013	0.077	0.045

Table 6

Calculated Mulliken atomic charges and Fukui functions for inhibitor C and maxima in bold, in gas and aqueous phases

Таблица 6. Расчетные атомные заряды Малликена и функции Фукуи для ингибитора С и максимумы, выделенные жирным шрифтом, в газовой и водной фазах

Atoms	Gas phase			Aqueous phase		
	f^+	f^-	f^0	f^+	f^-	f^0
C1	-0.015	0.085	-0.119	-0.01	0.096	-0.207
C2	0.064	0.105	0.048	0.085	0.123	0.057
C3	-0.005	0.016	-0.028	0.007	0.027	-0.038
C4	-0.197	-0.14	-0.265	-0.188	-0.12	-0.343
C8	-0.015	0.085	-0.119	-0.01	0.096	-0.018
C9	-0.197	-0.14	-0.265	-0.188	-0.12	-0.179
C10	-0.005	0.016	-0.028	0.007	0.027	-0.013
C11	0.065	0.105	0.048	0.085	0.123	0.076
C15	0.297	0.321	0.281	0.317	0.339	0.303
C16	0.297	0.321	0.281	0.317	0.339	0.296
N17	-0.209	-0.176	-0.242	-0.272	-0.249	-0.284
N18	-0.209	-0.176	-0.242	-0.272	-0.249	-0.304
N20	-0.297	-0.291	-0.312	-0.355	-0.343	-0.365
N21	-0.297	-0.291	-0.312	-0.355	-0.343	-0.381
O19	-0.495	-0.474	-0.502	-0.475	-0.461	-0.488

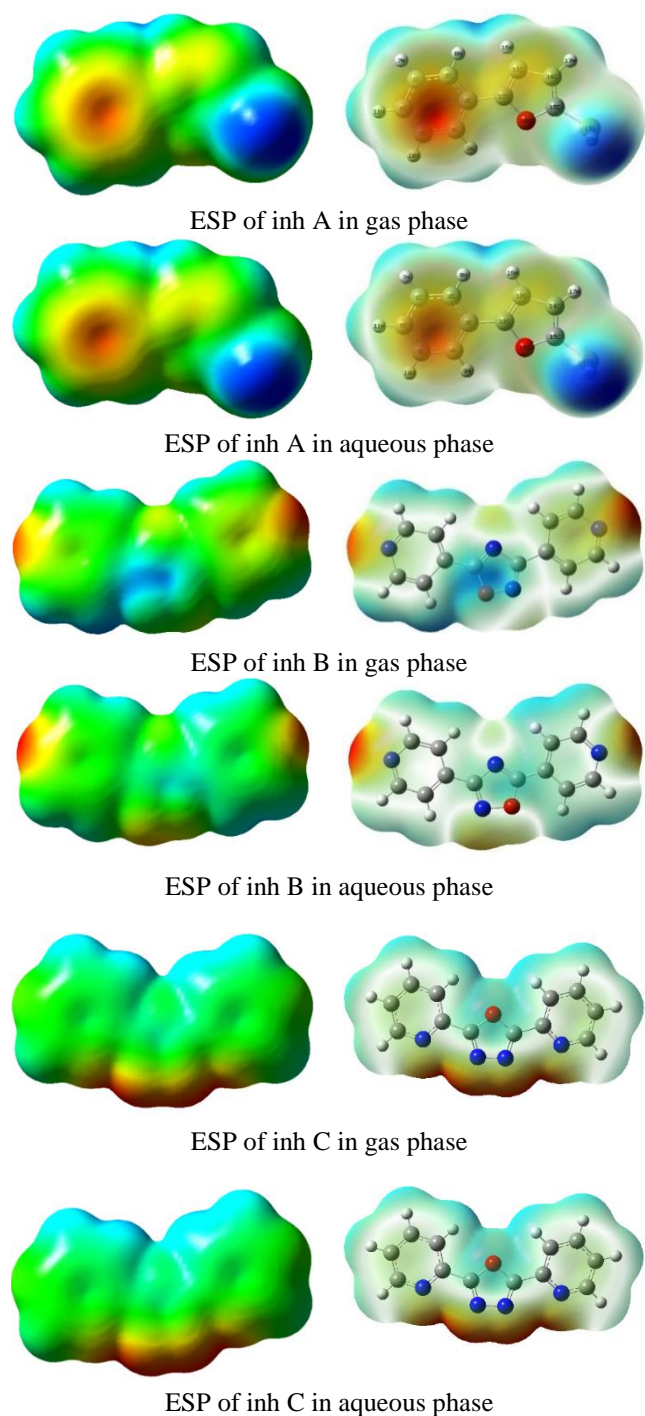


Fig. 5. Electrostatic potential map in gas and aqueous phases at B3LYP/6-311++ G (d,p) basis set

Рис. 5. Карта электростатического потенциала в газовой и водной фазах при базе B3LYP/6-311++ G (d,p)

Fig. 5 shows the electrostatic potentials (ESP) of chosen oxadiazoles from our work mapped on electron density surfaces. The minima and maximum are displayed in blue and red on these maps, respectively.

The negatively charged blue spots on the ESP maps are close to heteroatoms. These electron-rich locations would be ideal for adsorption to metal surfaces.

The molecular electrostatic potential (MEP) for compounds is also shown in Fig. 5. The MEP is a helpful identifier for determining whether locations in a molecule have proton affinity (charge regulated hard-hard interactions and the molecule's relative polarity). Higher negative charge, stronger electron density and higher affinity to a proton are shown by red regions. Blue regions have a higher positive charge, a lower electron density and a lower affinity for a proton. The red zone is near the Sulphur atom from the phenol group in inhibitor A while the blue region is near the Sulphur atoms from the mercaptan group in inhibitor A. The other two inhibitors B and C, the red regions located around heterocyclic atoms of (nitrogen atoms) from the oxadiazole groups.

MONTE CARLO SIMULATIONS

The Monte Carlo simulations aid in predicting the interaction of the inhibitor molecules with the surface of the metal [55]. It was used to induce the most stable low energy adsorption configurations of molecules A, B and C on the Fe (110) surface which are shown in Fig. 6. Because it is the most stable surface documented in the literature, the Fe (110) crystal surface was chosen for this simulation. A four-slab model was used to simulate the Fe (110) surface. Each layer in this model had 80 iron atoms, representing a (110) unit cell. For nonbonded interactions, a cut-off distance of 1.85 nm used with a spline transformation function (total energy, average total energy, van der Waals, electrostatic interactions, and intramolecular energy). Table 7 shows the results and characteristics, deformation energy, experimental efficiency %, stiff adsorption, comprising total adsorption and total energy. The energy produced when the relaxed adsorbate components deposited on the surface is related to the adsorption energy. The adsorption energy is the sum of the adsorbate component's deformation energies and rigid adsorption. Higher negative adsorption energy values represent a more stable and powerful interaction of a metal and an inhibitor molecule. The results in Table 7 can be shown that the negative values of furan and oxadiazoles derivative adsorption energies on the Fe (110) surface grow in the sequence $C > B > A$ which is similar to the experimental inhibitory efficiency values.

Table 7

The outputs and descriptors calculated by the Monte Carlo simulation for adsorption of A, B and C inhibitors on Fe (110) (in kcal mol⁻¹) and experimental inhibition efficiency

Таблица 7. Выходы и дескрипторы, рассчитанные с помощью моделирования Монте-Карло для адсорбции ингибиторов А, В и С на Fe (110) (в ккал/моль) и экспериментальная эффективность ингибирования

Inhibitor	Total energy (kcal mol ⁻¹)	Adsorption energy (kcal mol ⁻¹)	Rigid adsorption (kcal mol ⁻¹)	Deformation energy (kcal mol ⁻¹)	$\frac{dE_{ad}}{dN_i}$ (kcal mol ⁻¹)	Experimental efficiency %
A	25.011	-159.041	-3.174	-155.866	-159.041	78.4
B	49.322	-273.743	-4.183	-269.560	-273.743	93.97
C	48.042	-278.353	-4.356	-273.996	-278.353	95.3

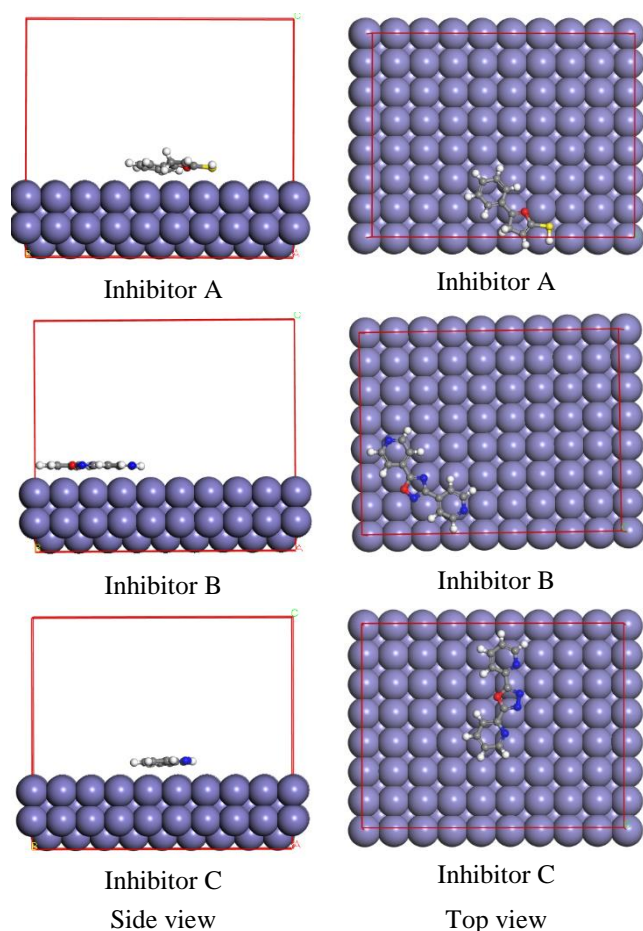


Fig. 6. Side and top views of the most stable low energy configurations for the adsorption of three inhibitors on Fe (110) interface attained using Monte Carlo simulations

Рис. 6. Виды сбоку и сверху на наиболее стабильные низкоэнергетические конфигурации адсорбции трех ингибиторов на границе раздела Fe (110), полученные с помощью моделирования методом Монте-Карло

EXPERIMENTAL REVIEW

A corrosion inhibitor is a chemical compound when introduced to an environment at modest concentrations, effectively reduces the corrosion rate. This improvement is expressed as a percentage, indicating the inhibitor's efficacy. Fig. 7 shows the results of IE % and corrosion rate derived from weight loss measurements for various concentrations of these components.

All of these chemicals have been found to prevent mild steel corrosion in 1 M HCl at all concentrations tested [6, 7, 14]. The IE for all of these drugs have been reported to increase with increasing inhibitor concentration. The adsorption of oxadiazoles on metal surfaces can occur either directly or by interacting directly with the donor-acceptor electrons on the heterocyclic molecule and the unoccupied d-orbitals on the iron surface atom, or by interacting with chloride or sulfate ions previously adsorbing them. The heterocyclic molecules could well be adsorbed on the surface as neutral molecules, causing water molecules to be displaced from the metal surface, electrons to be shared between nitrogen atoms and the metal surface. The organic compound's molecular structure is critical in synergistic inhibition. The highest synergistic inhibition is envisaged for an anion cation pair in which both ions have a significant proclivity for covalent binding. As a result, oxadiazole adsorption on the steel surface is larger than that of 1 M HCl solutions, resulting in increased inhibitory effectiveness. The pyridyl substituent occurs in aqueous acidic solutions as neutral species or as pyridinium cations that are maintained by an intramolecular hydrogen bond. The pyridinium substituent exerts an electron-drawing effect in this circumstance.

CONCLUSION

B3LYP density functional theory with 6-311++G(d, p) basis sets and the corrosion inhibition efficiency of furan and oxadiazoles against iron metal corrosion were predicted using a molecular dynamic modeling technique. Quantum chemical computations were performed for non-protonated and protonated species in gas and aqueous phases. In this study, a quantifiable link was discovered between electrophilicity (W), E_{HOMO} , electron charge transfer (ΔN_{max}), hardness (η), back-donation ($\Delta E_{\text{back-donation}}$) and inhibition efficiency for the compounds examined. All of these characteristics better describe the real experimental condition. When compared to other inhibitors, the inhibitor C has a superior nucleophilic character;

the greatest E_{HOMO} and the largest electron charge transfer (ΔN_{max}), highlighting its capabilities as an electron donor. It also has the highest hardness, as a result, a favorable back-donation charge. These findings were obtained for both phases, with and without the solvent effect. Despite the fact that a number of desirable quantum chemical characteristics correlate well with the inhibition effect of various inhibitors, there is still a lack of a straightforward relationship between others, such as E_{LUMO} , dipole, and inhibition efficiencies.

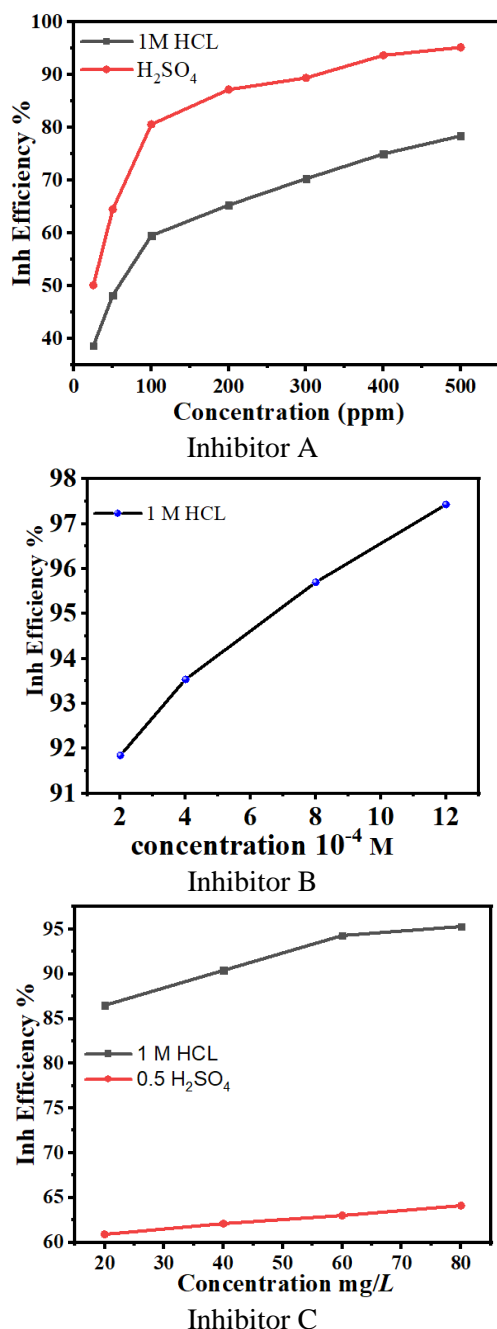


Fig. 7. Corrosion inhibition efficiency variation with rate concentrations [6, 7, 14]

Рис. 7. Изменение эффективности ингибирования коррозии в зависимости от концентрации [6, 7, 14]

Авторы заявляют об отсутствии конфликта интересов, требующего раскрытия в данной статье.

The authors declare the absence a conflict of interest warranting disclosure in this article.

REFERENCES
ЛИТЕРАТУРА

1. **Ebenso E.E., Isabirye D.A., Eddy N.O.** // *Int. J. Molec. Sci.* 2010. V. 11. N 6. P. 2473-2498. DOI: 10.3390/ijms11062473.
2. **Qadr H.M.** // *Atom Indonesia.* 2020. V. 46. N 1 // *Corrosion Sci.* 2000. 42(1). P. 127-146. DOI: 10.17146/aij.2020.923.
3. **Ju H., Ding L., Sun C., Chen J.-j.** // *Adv. in mater. sci. and eng.* 2015. P. 4875.
4. **El Ashry E.S.H., El Nemr A., Esawy S.A., Ragab S.** // *Electrochim. Acta.* 2006. 51(19). P. 3957-3968. DOI: 10.1016/j.electacta.2005.11.010.
5. **Bouanis M., Tourabi M., Nyassi A., Zarrouk A., Jama C., Bentiss F.** // *Appl. Surf. Sci.* 2016. 389. P. 952-966. DOI: 10.1016/j.apsusc.2016.07.115.
6. **Quraishi M., Sardar R.** // *Mater. chem. and phys.* 2003. 78(2). P. 425-431. DOI: 10.1016/S0254-0584(02)00299-7.
7. **Bentiss F., Traisnel M., Lagrenée M.** // *Corrosion sci.* 2000. 42(1). P. 127-146. DOI: 10.1016/S0010-938X(99)00049-9.
8. **Qadr H.M.** // *Russ. J. Non-Ferrous Metals.* 2021. V. 62. N 5. P. 561-567. DOI: 10.3103/S1067821221050096.
9. **Assad H., Kumar A.** // *J. Molec. Liq.* 2021. V. 344. P. 117755. DOI: 10.1016/j.molliq.2021.117755.
10. **Solmaz R.** // *Corrosion Sci.* 2010. V. 52. N 10. P. 3321-3330. DOI: 10.1016/j.corsci.2010.06.001.
11. **Saha D., Kienbaum M.J.** // *Micropor. Mesopor. Mater.* 2019. V. 287. P. 29-55. DOI: 10.1016/j.micromeso.2019.05.051.
12. **Gece G.** // *Corrosion Sci.* 2011. V. 53. N 12. P. 3873-3898. DOI: 10.1016/j.corsci.2011.08.006.
13. **Mohammad Q.H., Maghdid H.A.** // *Радиоэлектроника. Наносистемы. Информ. технологии.* 2020. Т. 12. № 4. С. 451-456.
14. **Mohammad Q.H., Maghdid H.A.** // *Radioelektr. Nanosystemy. Inform. Tekhnol.* 2020. V. 12. N 4. P. 451-456 (in Russian).
15. **Outirite M., Lagrenée M., Lebrini M., Traisnel M., Jama C., Vezin H.** // *Electrochim. Acta.* 2010. V. 55. N 5. P. 1670-1681. DOI: 10.1016/j.electacta.2009.10.048.
16. **Alamiery A.A.** // *Mater. Sci. En. Technol.* 2021. V. 4. P. 263-273. DOI: 10.1016/j.mset.2021.07.004.
17. **Hiwa M.Q.** // *Вестн. Москов. гос. техн. ун-та. Сер. «Естеств. науки».* 2020. Т. 2. № 89. С. 117-125.
18. **Hiwa M.Q.** // *Vest. Moscov. Gos. Tekh. Un-ta. Ser. Estesstv. Nauki.* 2020. V. 2. N 89. P. 117-125 (in Russian).
19. **Kuznetsov Y.I., Kazansky L.** // *Russ. Chem. Rev.* 2008. V. 77. N 3. P. 219. DOI: 10.1070/RC2008v077n03ABEH003753.
20. **Mamand D.M., Awla A.H., Anwer T.M.K., Qadr H.M.** // *Chimica Techno Acta.* 2022. V. 9. N 2. P. 20229203. DOI: 10.15826/chimtech.2022.9.2.03.
21. **Verma C., Olasunkanmi L., Ebenso E.E., Quraishi M.** // *J. Molec. Liq.* 2018. V. 251. P. 100-118. DOI: 10.1016/j.molliq.2017.12.055.
22. **Mamand D.M.** Investigation of spectroscopic and optoelectronic properties of benzimidazobenzophenanthroline molecule: Fen Bilimleri Enstitüsü. 2020.
23. **Qadr H.M.** // *Annals of "Dunarea de Jos" University of Galati Fascicle IX, Metallurgy and Materials Science.* 2020. V. 43. N 4. P. 13-16. DOI: 10.35219/mms.2020.4.02.

22. Frisch A. Gaussian 09W Reference. Wallingford, USA. 470 p. 2009.
23. Meunier M. Introduction to materials studio2012: EDP Sciences.
24. Ahmed S.K., Ali W.B., Khadom A.A. // *Internat. J. Ind. Chem.* 2019. V. 10. N 2. P. 159-173. DOI: 10.1007/s40090-019-0181-8.
25. Shahraki M., Dehdab M., Elmi S. // *J. Taiwan Inst. Chem. Eng.* 2016. V. 62. P. 313-321. DOI: 10.1016/j.jtice.2016.02.010.
26. Erdoğan Ş., Safi Z.S., Kaya S., Işın D.Ö., Guo L., Kaya C. // *J. Molec. Struct.* 2017. V. 1134. P. 751-761. DOI: 10.1016/j.molstruc.2017.01.037.
27. Mamand D.M., Rasul H.H., Omer P.K., Qadr H.M. // *Condens. Matter Interphases.* 2022. V. 24. N 2. P. 227-242. DOI: 10.17308/kcmf.2022.24/9263.
28. Cammi R., Mennucci B. // *J. Chem. Phys.* 1999. V. 110. N 20. P. 9877-9886. DOI: 10.1063/1.478861.
29. Rodríguez-Valdez L.M., Martínez-Villafañe A., Glossman-Mitnik D. // *J. Molec. Struct.: THEOCHEM.* 2005. V. 713. N 1-3. P. 65-70. DOI: 10.1016/j.theochem.2004.10.036.
30. Wazzan N.A., Al-Qurashi O.S., Faidallah H.M. // *J. Molec. Liq.* 2016. V. 223. P. 29-47. DOI: 10.1016/j.molliq.2016.07.146.
31. Qadr H.M., Mamand D.M. // *J. Bio Tribo-Corrosion.* 2021. V. 7. N 4. P. 1-8. DOI: 10.1007/s40735-021-00566-9.
32. Tarrad S.N., Hussain S.A., Al-Asady F.H. // *AIP Conf. Proc.* 2020.
33. Kaya S., Kaya C., Guo L., Kandemirli F., Tüzün B., Uğurlu İ. // *J. Molec. Liq.* 2016. V. 29. P. 497-504. DOI: 10.1016/j.molliq.2016.03.042.
34. Mamand D.M., Anwer T.M.K., Qadr H.M. // *Oxid. Commun.* 2022. V. 45. N 4. P. 600-627.
35. Sastri V., Perumareddi J. // *Corrosion.* 1997. V. 53. N 08. 35 p. DOI: 10.5006/1.3290294.
36. Eddy N.O., Stoyanov S.R., Ebenso E.E. // *Int. J. Electrochem. Sci.* 2010. V. 5. P. 1127-1150.
37. Obot I., Kaya S., Kaya C., Tüzün B. // *Physica E: Low-Dimens. Syst. Nanostruct.* 2016. V. 80. P. 82-90. DOI: 10.1016/j.physe.2016.01.024.
38. Popova A., Christov M., Deligeorgiev T. // *Corrosion.* 2003. V. 59. N 09. P. 756-764. DOI: 10.5006/1.3277604.
39. Mamand D.M., Anwer T.M.K., Qadr H.M. // *J. Indian Chem. Soc.* 2023. V. 100. N 6. P. 101018. DOI: 10.1016/j.jics.2023.101018.
40. Obi-Egbedi N., Obot I., El-Khaiary M., Umoren S., Ebenso E. // *Int. J. Electrochem. Sci.* 2011. V. 6. N 1. P. 5649-5675.
41. Avery S.V., Tobin J.M. // *Appl. Environ. Microbiology.* 1993. V. 59. N 9. P. 2851-2856. DOI: 10.1128/aem.59.9.2851-2856.1993.
42. Singh P., Srivastava V., Quraishi M. // *J. Molec. Liq.* 2016. V. 216. P. 164-173. DOI: 10.1016/j.molliq.2015.12.086.
43. Pearson R.G. // *Proc. Nat. Acad. Sci.* 1986. V. 83. N 22. P. 8440-8441. DOI: 10.1073/pnas.83.22.8440.
44. Mamand D. // *J. Phys. Chem. Funct. Mater.* 2019. V. 2. N 2. P. 77-86.
45. Mamand D.M., Qadr H.M. // *Protect. Metals Phys. Chem. Surf.* 2021. V. 57. N 5. P. 943-953. DOI: 10.1134/S207020512105018X.
46. Ebenso E.E., Arslan T., Kandemirli F., Caner N., Love I. // *Int. J. Quant. Chem.* 2010. V. 110. N 5. P. 1003-1018. DOI: 10.1002/qua.22249.
47. Bereket G., Hür E., Öğretir C. // *J. Molec. Struct.: THEOCHEM.* 2002. V. 578. N 1-3. P. 79-88. DOI: 10.1016/S0166-1280(01)00684-4.
48. Abreu-Quijano M., Palomar-Pardavé M., Cuán A., Romero-Romo M., Negrón-Silva G., Álvarez-Bustamante R. // *Int. J. Electrochem. Sci.* 2011. V. 6. № 9. P. 3729-3742.
49. Mamand D.M., Anwer T.M., Qadr H.M., Mussa C.H. // *Russ. J. Gen. Chem.* 2022. V. 92. № 9. P. 1827-1838. DOI: 10.1134/S1070363222090249.
50. Gómez B., Likhanova N.V., Domínguez-Aguilar M.A., Martínez-Palou R., Vela A., Gazquez J.L. // *J. Phys. Chem. B.* 2006. V. 110. N 18. P. 8928-8934. DOI: 10.1021/jp057143y.
51. Chalasinski G., Szczesniak M.M. // *Chem. Rev.* 1994. V. 94. N 7. P. 1723-1765. DOI: 10.1021/cr00031a001.
52. Qadr H.M. // *Phys. Particles Nuclei Lett.* 2021. V. 18. N 2. P. 185-189. DOI: 10.1134/S1547477121020151.
53. Pearson R.G. // *J. Am. Chem. Soc.* 1963. V. 85. N 22. P. 3533-3539. DOI: 10.1021/ja00905a001.
54. Mamand D.M., Qadr H.M. // *Russ. J. Phys. Chem. A.* 2022. V. 96. N 10. P. 2155-2165. DOI: 10.1134/S0036024422100193.
55. Frenkel D., Smit B., Ratner M.A. Understanding molecular simulation: from algorithms to applications. San Diego: Acad. Press. 1996.

Поступила в редакцию 30.01.2023

Принята к опубликованию 01.06.2023

Received 30.01.2023

Accepted 01.06.2023